Received: 6 November 2019 | Revised: 9 December 2019 | Accepted: 29 December 2019

DOI: 10.1111/jace.16988

ORIGINAL ARTICLE

Journal of the American Ceramic Society

Porous SiOC monoliths with catalytic activity by in situ formation of Ni nanoparticles in solution-based freeze casting

Daniel Schumacher[1] | **Michaela Wilhelm**[1] | **Kurosch Rezwan**[1,2]

[1]Advanced Ceramics, University of Bremen, Bremen, Germany

[2]MAPEX—Centre for Materials and Processes, University of Bremen, Bremen, Germany

Correspondence
Michaela Wilhelm, Advanced Ceramics, University of Bremen, Bremen, Germany.
Email: mwilhelm@uni-bremen.de

Funding information
Deutsche Forschungsgemeinschaft, Grant/Award Number: 1860

Abstract

Micro- and macroporous monoliths with in situ formed nickel nanoparticles were prepared for the first time by the combination of solution-based freeze casting and preceramic polymers (methyl polysiloxane). This one-step process results in macroporous monoliths composed of microporous and catalytic active nickel-containing polymer-derived ceramic. Four different complexing and cross-linking siloxanes with amino functionality were screened for their ability to create small nickel particles. TEM analysis confirmed 3-aminopropyltriethoxysilane being most efficient. High BET-specific surface areas of 344-461 $m^2\ g^{-1}$ were achieved. Increased ratio of complexing groups to nickel improves the dispersion of nickel to (3.61 ± 1.49) nm. The nickel size dependence of conversion (maximum 0.49) and CH_4 selectivity (maximum 0.74) in CO_2 methanation emphasizes the importance of controlling the nickel size. The hydrophobic surface characteristic is hypothesized to be the main reason polymer-derived catalysts having better catalytic activity compared with nickel-impregnated silica. The promising catalytic activity combined with the versatile freeze casting process can prospectively address heat- and mass-transfer considerations in heterogeneous monolith catalysis.

KEYWORDS

catalyst/catalysis, polymer precursor, porous materials, solution-based freeze casting

1 | INTRODUCTION

Nickel catalysts are the most intense studied catalysts for CO_2 methanation, also called Sabatier reaction ($CO_2 + 4H_2 \rightarrow CH_4 + 2H_2O$, $\Delta H_0 = -164$ kJ mol^{-1}).[1] New concepts for energy storage such as "power-to-gas" and "power-to-liquid" require reactions such as CO_2 methanation in order to generate methane and fuels from CO_2 and hydrogen.

Although, noble metal catalysts (Rh, Ru, Pd) show superior performance especially at low temperatures, their high costs and limited abundance restrict their application in industrial processes compared with transitions metals (Ni, Fe, Co).[1–5] In heterogeneous catalysis, the support is very important to the performance with dispersing the active metal being its major role. High metal loading often results in aggregated metal particles with reduced catalytic activity.[4] Since water is a major product in CO_2 methanation a hydrophobic surface is claimed to avoid blocking of adsorption sites by water molecules.[6] Furthermore, weak interaction between the metal and the support was found to increase the activity due to a good reducibility of the metal.[7]

This is an open access article under the terms of the Creative Commons Attribution License, which permits use, distribution and reproduction in any medium, provided the original work is properly cited.
© 2020 The Authors. *Journal of the American Ceramic Society* published by Wiley Periodicals, Inc. on behalf of American Ceramic Society (ACERS).

The support influences the adsorption capability of the metal phase, its morphology, the metal-support interaction, and finally the catalytic properties.[8] The preparation method effects the dispersion of the active phase and the metal-support interaction and hence strongly influences the overall catalytic behavior.[9] Numerous processes to prepare heterogeneous catalysts such as impregnation, sol-gel methods, co-precipitation, and hydrothermal processes have been tested.[1,10]

Besides them, in situ formation of metal nanoparticles in a polymer-derived ceramics (PDCs) matrix proofed to result in small and very homogeneously distributed metal particles.[11–13] A great variety of metals such as nickel, iridium, platinum, palladium, iron, cobalt, copper, silver, and gold were incorporated in PDC matrixes.[13–16] However, only some metal-containing systems were fabricated for heterogeneous catalysis. Compared with conventional preparation processes, the in situ formation of metal particles and their reduction during inert-gas pyrolysis prevents the generation of hardly reducible oxides.[16] Furthermore, it has turned out that a complexing agent is strongly influencing the final metal size by complexing the nickel ions with, for example, amino groups. Complexing siloxanes were reported to be very efficient in creating a small and homogenously distributed nickel nanoparticles.[12,13] In addition, varying the process parameters such as pyrolysis temperature and chemical composition allows for the adjustment of properties like porosity, surface characteristics, and metal dispersion.[17]

Apart from the widely used reflux synthesis or polymeric shaping techniques, solution-based freeze casting of preceramic polymers allows for the generation of porous PDCs monoliths.[18] In solution-based freeze casting, pores are formed by thermally induced phase separation of a homogenous polymeric solution during freezing. After completely frozen, the solvent is removed by sublimation resulting in a porous body with a pore structure reflecting the solvent crystals. The choice and the amount of the cross-linking agent has to be carefully adjusted in order to ensure sufficient cross-linking but prevent gelation before freezing.[18] Using cross-linking agents (CLAs) with amino groups adds the functionality of complexing metal ions to the cross-linking agent. Although metal-containing PDCs have shown potential for catalytic applications and the fact that monolithic heterogeneous catalysis is supposed to overcome heat transport limitations no investigations were carried out on porous metal-containing PDC monoliths, yet. Prior to optimizing such a monolithic catalyst in terms of pore structure, it has to be guaranteed that the underlying principles and processes of producing a porous metal-containing PDC monolith are understood.

In this study, micro- and macro-porous catalytic active monoliths are prepared by solution-based freeze casting of methyl polysiloxane and in situ formation of nickel nanoparticles. In order to find an optimized cross-linking agent within the restrictions of solution-based freeze casting, four different siloxanes with amino functionalities are screened for their ability to generate small and homogenous distributed nickel nanoparticles. Further variations were carried out for the most effective cross-linking agent. The amino to nickel ratio was increased, the pyrolysis temperature was altered and the nickel precursor was changed.

2 | EXPERIMENTAL SECTION

2.1 | Materials

Ni-containing porous ceramic monoliths were prepared by solution-based freeze casting. A commercial methyl polysilsesquioxane (MK, Silres® MK, Wacker Chemie AG) and tert-butyl alcohol (TBA, >99%; Thermo Fisher GmbH) were used as preceramic polymer and solvent, respectively. Nickel(II) acetylacetonate (NiA, >95%, Sigma-Aldrich) and nickel(II) nitrate hexahydrate (NiN, 99.99%, Sigma-Aldrich) acted as nickel precursor. NiN was chosen as a reference precursor. While NiN is reported to suffer from problems such as sintering and redistribution, such behavior is not known for NiA.[8,19] Additionally, the better solubility of NiA in organic solvents provides a better compatibility with the presented approach of using polymeric solutions. To ensure complexing of nickel ions and provide cross-linking of the polymeric network, 3-aminopropyldiethoxymethylsilane (APD, Sigma-Aldrich) 3-aminopropyltriethoxysilane (AP, abcr GmbH), 2-aminoethyl-3-aminopropyltrimethoxysilane (AE, abcr GmbH) and Tetramethylethylenediamine (TMEDA, Sigma-Aldrich) were used. The complexing and CLAs were chosen according to their ratio between complexing groups ($R'NH_2$, R'_2NH, and R'_3N) and cross-linking active groups (OR). The ratio ranges from 0 (TMEDA) to 2/3 (AE) with APD (1/2) and AP (1/3) being in between. Chemical structures and indication of complexing and cross-linking functionalities for all CLAs are shown in Figure 1. All raw materials were used without further treatment or purification.

2.2 | Freeze casting

The preparation of porous monolithic Ni-containing samples by solution-based freeze casting is depicted in Figure 1. The overall solid loading was kept constant at 30 wt%. Whereby, the preceramic polymer, the Ni precursor, and the CLA counted as solid fraction. For the preceramic polymer solution, MK was added to TBA under vigorous stirring. Meanwhile, the metal-containing solution was prepared by adding the metal precursor and the CLA to TBA. Subsequently, the preceramic polymer solution was added to the metal-containing solution.

The solution was poured into a mold, which consists of a PVC bottom and an aluminum rod with an inner diameter of 20 mm and a height of 60 mm. A silicon coated PET film (Hostaphan RN 30 2SLK, Mitsubishi Polyester Film GmbH) was used as separation layer between solution and rod. After casting, the mold was transferred to a freezer at −20°C for 72 hours. After demolding, the solvent was sublimated in a freeze dryer for 72 hours at −20°C shelf temperature and a pressure of 1000 µbar. Finally, the monoliths were pyrolyzed at 500 or 600°C under the flow of nitrogen with a heating rate of 2 K/min and a dwelling time of 4 hours. Where required the monoliths were milled and subsequently sieved with a mesh size of 200 µm. The samples were labeled according to: [nickel precursor] [ratio of complexing groups to nickel ions] [CLA]/[pyrolysis temperature in °C]. Table 1 gives an overview of all samples and their compositions. For comparison of the catalytic activity, a reference catalyst was prepared by wet impregnation of commercial silica (1 µm, AngstromSphere; Fiber Optic Center Inc) with nickel(II) nitrate hexahydrate (99.99%, Sigma-Aldrich). Subsequently, the catalyst was dried at 70°C for 24 hours and pyrolyzed at 600°C.

2.3 | Materials characterization

The pore structure of the monolithic samples was investigated using scanning electron microscopy (SEM, field-emission SEM SUPRA 40; Zeiss) operating at 10.00 kV. Hg intrusion measurements were conducted to reveal the open porosity and the mean pore window diameter (Pascal 140/440; POROTEC GmbH). Specific surface area (SSA) was determined by evaluating nitrogen adsorption isotherms

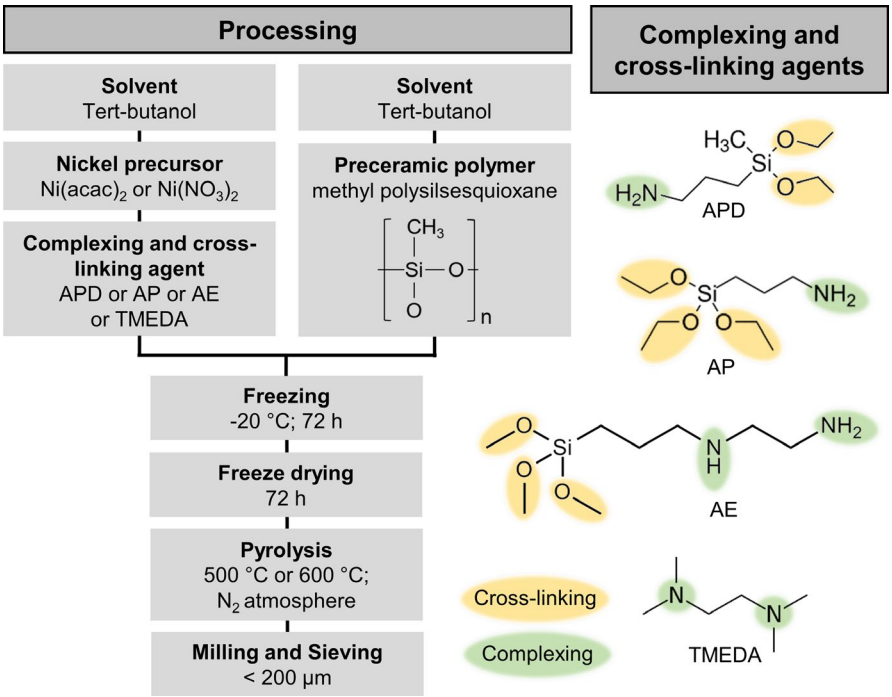


FIGURE 1 Process scheme and overview of complexing and cross-linking agents with indication of cross-linking and complexing functionalities [Color figure can be viewed at wileyonlinelibrary.com]

TABLE 1 Denotation, composition, and pyrolysis temperatures applied for all samples

Denotation	Ni precursor	Ratio complexing groups/Ni	Complexing agent	Pyrolysis temperature (°C)	Final metal loading (wt%)[a]
NiA2APD/600	$Ni(acac)_2$	2	APD	600	3.62
NiA2AP/600	$Ni(acac)_2$	2	AP	600	4.19
NiA2AE/600	$Ni(acac)_2$	2	AE	600	3.69
NiA2TMEDA/600	$Ni(acac)_2$	2	TMEDA	600	3.48
NiA4AP/600	$Ni(acac)_2$	4	AP	600	3.25
NiA4AP/500	$Ni(acac)_2$	4	AP	500	3.10
NiN4AP/600	$Ni(NO_3)_2$	4	AP	600	3.73
Ref Ni/SiO_2	$Ni(NO_3)_2$	—	—	600	5.00[b]

[a]According to TGA measurements.

[b]Calculated based on composition.

according to BET theory (Belsorp-Max, Bel Japan Inc). Measurements of vapor adsorption were performed by placing open vessels with ≈ 1 g samples in closed Erlenmeyer flasks filled with liquids for 24 hours. The adsorption of the liquids water and heptane was a measure of hydrophilic and hydrophobic surface characteristic, respectively. The liquids were at equilibrium with their vapor phase at 20°C and atmospheric pressure. Prior to the measurement, the samples were dried at 70°C for 24 hours. Final metal loading in pyrolyzed samples was determined by thermogravimetric analysis in N_2 atmosphere (STA 503; Bähr Thermoanalyse GmbH) assuming no loss of nickel during heat treatment. X-ray diffraction (XRD 3003; Seifert) was used to investigate the phase composition of pyrolyzed samples. Scans were performed Cu-Kα radiation in a range between $2\theta = 5°$-$80°$ at a step width of 0.025° and a time per step of 8 seconds. The size and dispersion of nickel nanoparticles was determined by the analysis of TEM images (Titan 80/300; FEI). To ensure statistically relevant results a minimum of nine images were captured of each sample and the average particle size of a minimum of 120 nickel particles was used for comparison. CO_2 methanation in a fixed bed reactor was used as probe reaction to investigate the catalytic activity. Fifty milligrams of sample was mixed with 300 mg of inert filler (Al_2O_3). The tubular reactor has an inner diameter of 9 mm and the total flow was set to 50 mL/min, which gives a weight hourly space velocity of 60 L g_{cat}^{-1} h^{-1} Whereby, the stoichiometric ratio of feed gases was $H_2/CO_2/Ar = 16/4/5$. Activation was conducted at 440°C for 10 hours at a flow of 20 mL/min H_2 with heating and cooling rates of 2 K/min. To ensure steady state, the temperature was hold at each measurement point for 40 minutes before the product stream was analyzed. Gas chromatography (5890 Series II; Hewlett-Packard) equipped with a thermal detector and a column to detect CH_4, CO, and CO_2 (Carboxen 1006 PLOT, 30 m × 0.53 mm; Supelco) were used to determine the CO_2 conversion X_{CO_2}(a), the CH_4 yield Y_{CH_4} (b) as well as the CH_4 selectivity S_{CH_4} (c) according to following equations based on the assumption of carbon conservation:

$$X_{CO_2} = 1 - \frac{c_{CO_{2,out}}}{c_{CO_{2,\,out}} + c_{CH_{4,out}} + c_{CO_{out}}} \quad (1)$$

$$Y_{CH_4} = \frac{c_{CH_{4,out}}}{c_{CO_{2,out}} + c_{CH_{4,out}} + c_{CO_{out}}} \quad (2)$$

$$S_{CH_4} = \frac{Y_{CH_4}}{X_{CO_2}} \quad (3)$$

Additionally, the stability was exemplary evaluated on the sample NiA4AP/600 at 400°C for 10 hours under reaction conditions.

3 | RESULTS

3.1 | Pore structure

SEM images were recorded and Hg intrusion experiments were conducted to investigate the pore structure of monolithic samples. Figure 2A-G shows the characteristic pore structure. The samples with a complexing group to Ni ratio of Figure 2A-D exhibit a prismatic like pore morphology with a pronounced orientation of the pore channels in radial direction. Orientation of the pores originates from the direction of freezing since the solvent crystals grow in the direction of heat transfer.[20] Additionally, Hg intrusion measurements reveal mean pore window diameters of 8.2-15.1 μm as it can be seen in Figure S1. Changing the ratio of complexing groups to Ni from 2 to 4 results in a more unordered pore morphology with a channel like backbone superimposed by filigree details and interruptions of channels. Besides changes in the pore morphology, the mean pore window diameters significantly increase to values of 24.4-29.1 μm. Preliminary test revealed that the addition of metal precursors is not the reason for the change in pore morphology. Rather, these preliminary tests show that the increased amount of CLA is supposed to alter the pore morphology. Figure S2 clearly shows the change in pore morphology with increasing amount of the CLA AP. This finding indicates that high amounts of CLAs interfere the regular crystal growth. Figure 2H shows a highly porous particle before the catalysis test.

3.2 | SSA and surface characteristic

In addition to the pore structure, SSA and the surface chemistry with regards to hydrophilicity/hydrophobicity are important properties. Nitrogen adsorption isotherms were recorded to evaluate the SSA according to BET theory. Figure 3 depicts the BET-SSA. All samples exhibit type I isotherms indicating the presence of micropores as it can be seen in Figure S3. This is in accordance with the relatively high BET SSA in the range of 343-461 m^2 g^{-1}. Micropores are formed during pyrolysis by the release of gaseous decomposition products. Mainly the decomposition of the CLAs and of the methyl group of MK contribute to the formation of micropores. Besides its positive effect in catalyzing the cross-linking, nickel is supposed to enhance the polymer-to-ceramic conversion. Consequently, the decomposition of the methyl group in MK is shifted to lower temperatures as it was observed in previous TGA measurements. This behavior

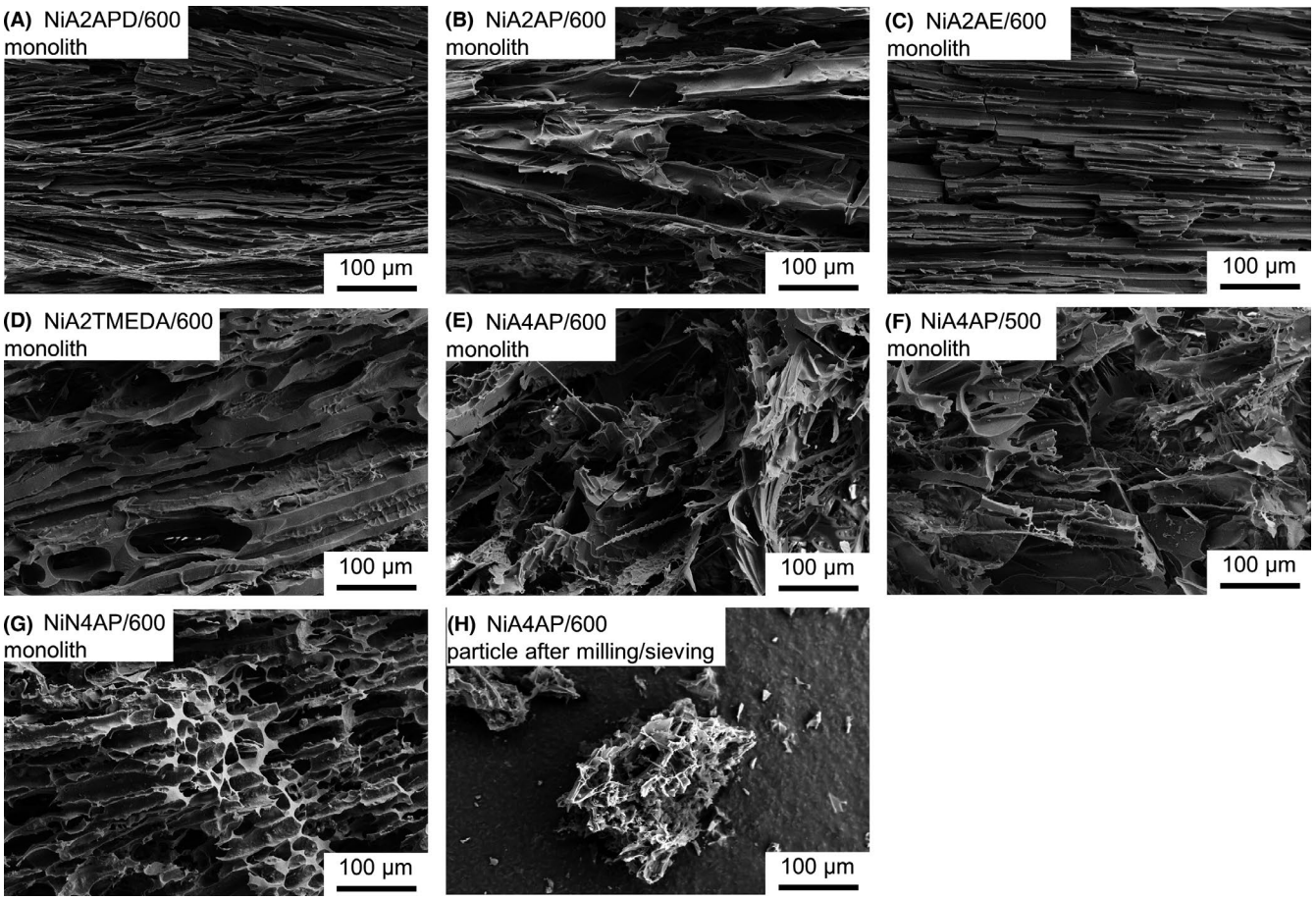


FIGURE 2 SEM images of the characteristic pore structure (A-G) of all samples and exemplary SEM image of a particle of sample AP4NiA/600 used in catalysis measurement (H)

of polysiloxanes has been reported in literature for nickel as well as for other metals.[11,17,21,22] Studies using similar precursors found comparable BET SSA.

All samples with NiA as nickel precursor and a pyrolysis temperature of 600°C show very similar BET SSA of 401-410 $m^2\ g^{-1}$. Hence, different CLAs are not influencing the BET SSA. Furthermore, also the ration between complexing groups and nickel ions does not affect the BET SSA as NiA2AP/600 and NiA4AP/600 show no significant difference in surface area. Reducing the pyrolysis temperature from 600 to 500°C leads to a rise in BET SSA from 403 to 461 $m^2\ g^{-1}$. After the formation of micropores, further increase in the pyrolysis temperature typically results in the collapse of micropores as it is reported in literature.[23,24] Changing the nickel precursor from NiA to NiN reduces the BET SSA from 403 to 344 $m^2\ g^{-1}$. In contrast to the polymer-derived catalysts, the reference catalyst shows a type III isotherm with a BET SSA of 2 $m^2\ g^{-1}$ as it can be seen in Figure S2.

Apart from the SSA, the surface characteristic in terms of hydrophilicity/hydrophobicity is important when it comes to the interaction of molecules with the surface. Vapor adsorption measurements were performed with water and heptane as probe molecules for polar and unpolar surface characteristics, respectively. Figure 4 shows the ratio of adsorbed water to adsorbed heptane at 22°C. Samples with ratios <1 are considered to be hydrophobic. In contrast, a ratio of >1 indicates hydrophilic

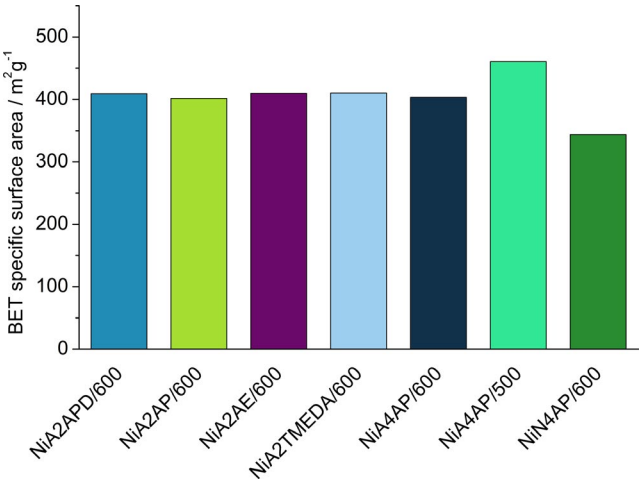


FIGURE 3 BET-specific surface area determined by N_2 adsorption for different cross-linking agents, Ni precursors, and pyrolysis temperatures [Color figure can be viewed at wileyonlinelibrary.com]

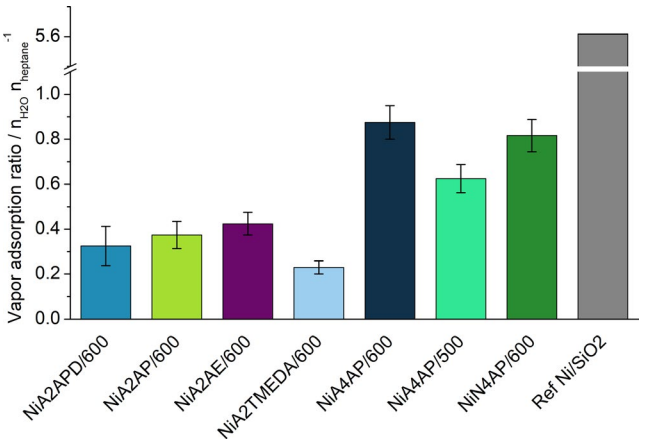


FIGURE 4 Vapor adsorption ratio of H_2O to heptane at 22°C for different cross-linking agents, Ni precursors, and pyrolysis temperatures [Color figure can be viewed at wileyonlinelibrary.com]

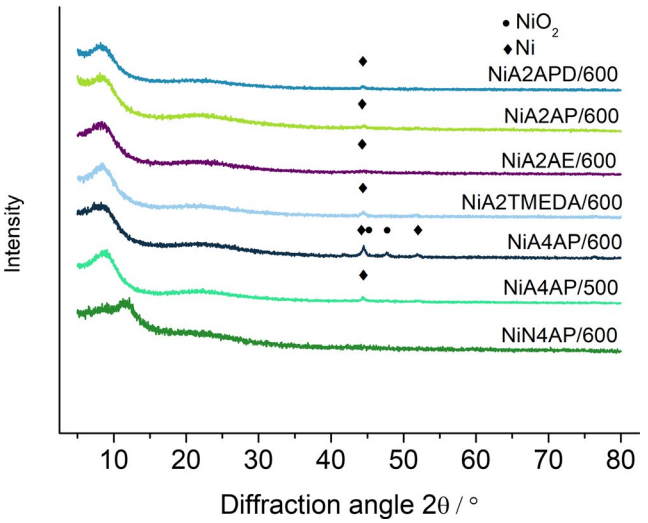


FIGURE 5 X-ray diffractograms of samples with different cross-linking agents, Ni precursors, and pyrolysis temperatures [Color figure can be viewed at wileyonlinelibrary.com]

surface characteristic. All samples exhibit a hydrophobic behavior. Two groups of samples can be distinguished: the one with a complexing group to Ni ratio of 2 and the other one with the increased ratio of 4. It is known that the metal-free preceramic polymer MK pyrolyzed at 600°C itself is hydrophobic.[25] Since, the amine groups of the CLA are almost completely decomposed at 600°C Si-containing CLAs mainly add additional hydrophilic SiO units to the pyrolyzed structure.[26,27] The samples NiA2APD/600 and NiA2AP/600 exhibit one Si atom per complexing amine group. In contrast, NiA2AE/600 includes only 0.5 Si atoms per amine group and NiA2TEMDA/600 has no Si atoms at all. Therefore, the ratio of vapor adsorption is similar for NiA2APD/600, NiA2AP/600, and NiA2AE/600 reaching values of 0.32 ± 0.09, 0.37 ± 0.06, and 0.42 ± 0.05, respectively. In contrast, NiA2TEMDA/600 without additional hydrophilic SiO units provided by TMEDA exhibits the lowest hydrophilicity with a value of 0.23 ± 0.03. Following this argumentation, samples with higher amount of CLA such as NiA4AP/600, NiA4AP/500, and NiN4AP/600 show values of 0.87 ± 0.07, 0.62 ± 0.06, and 0.82 ± 0.07, respectively. Decreasing the pyrolysis temperature from 600 to 500°C results in less decomposition of organic groups and consequently in an increased hydrophobicity as it can be seen comparing NiA4AP/600 and NiA4AP/500.[25] No significant influence of the nickel precursor on the surface characteristic can be seen when comparing NiA4AP/600 with NiN4AP/600. According to TGA measurements both anions, for example, nitrate and acetylacetonate are decomposed at 500°C. Hence, it can be assumed that they do not have an influence on the final surface characteristics.

3.3 | Characterization of Ni nanoparticles

XRD measurements were performed to gain knowledge on the crystal phase composition. Figure 5 shows X-ray diffractograms of pyrolyzed samples. In all samples, broad reflections between 10° and 30° 2θ are present indicating the formation of a Si-based amorphous phase as it is characteristic for polysiloxanes at this pyrolysis temperature. Additionally, the peaks found around 45°, 52°, and 77° 2θ are representing the cubic Ni structure. For NiA4AP/600 also peaks correlated with NiO_2 can be detected. NiO_2 formation is assumed also in the other samples, but cannot be detected by XRD due to low intensity of peaks. The absence of diffraction peaks related to other secondary phases such as Ni_2Si confirms that the samples are single phase consisting after pyrolysis. Metallic nickel particles are formed during pyrolytic conversion of the nickel-containing polysiloxanes under inert atmosphere. Released decomposition products such as hydrocarbons and hydrogen are creating reductive conditions within the sample and its pore network.[16] The absence of significant Ni peaks in NiN4AP/600 due to superimposition by the background indicate very small nickel particles.

The presence and distribution of nickel nanoparticles were investigated by image analysis of TEM images. Figure 6 depicts representative TEM images and the average nickel size of all samples after pyrolysis (Figure 6A-G) and of NiA4AP/600 after 10 hours stability test at 400°C (Figure 6H). When considering the samples with a complexing group to nickel ratio of 2, NiA2APD/600 and NiA2AP/600 exhibit similar nickel particle sizes of (4.94 ± 4.42) nm and (3.91 ± 3.30) nm, respectively. Using AE and TMEDA as CLA lead to an increase in nickel particle size to (7.15 ± 6.65) nm and (12.4 ± 10.45) nm, respectively. While increasing the complexing group to nickel ratio from 2 to 4 only slightly decreases the nickel particle size, it significantly reduces the nickel particle size distribution from (3.91 ± 3.30) nm to (3.61 ± 1.49) nm as it can be

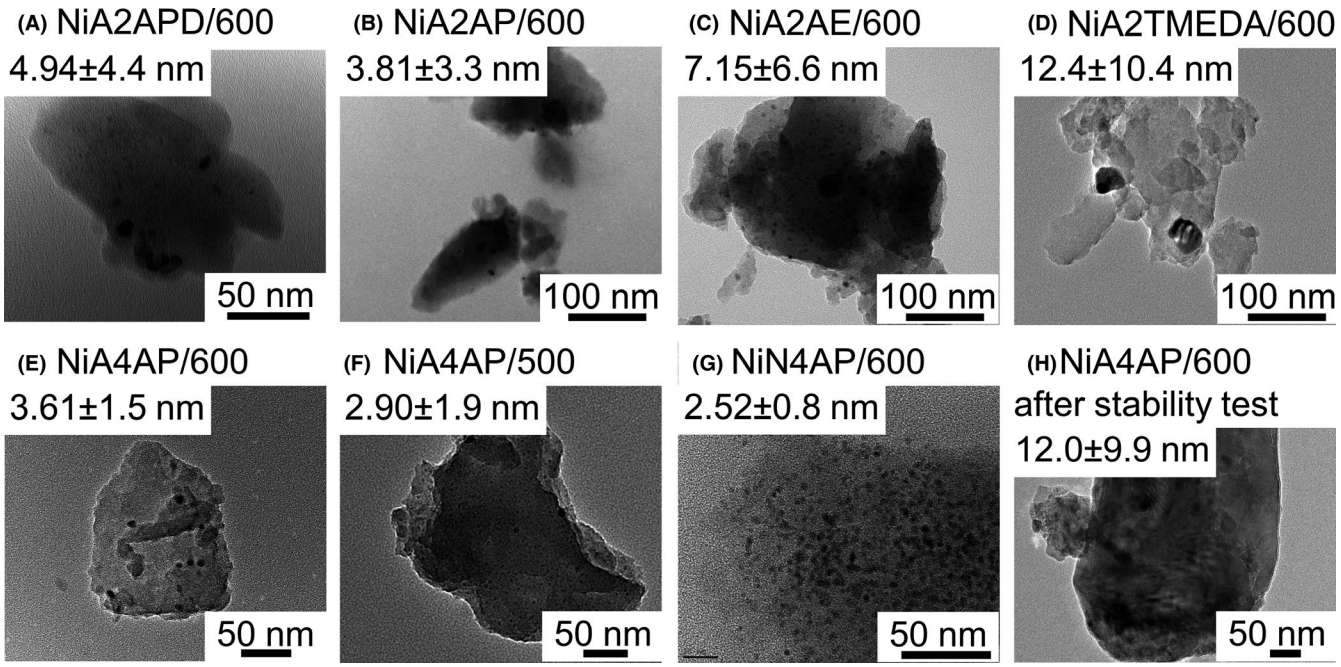


FIGURE 6 TEM images and Ni particle size of freshly pyrolyzed samples with different cross-linking agents, Ni precursors and pyrolysis temperatures (A–G) and sample after 10 h on stream at 400°C (H)

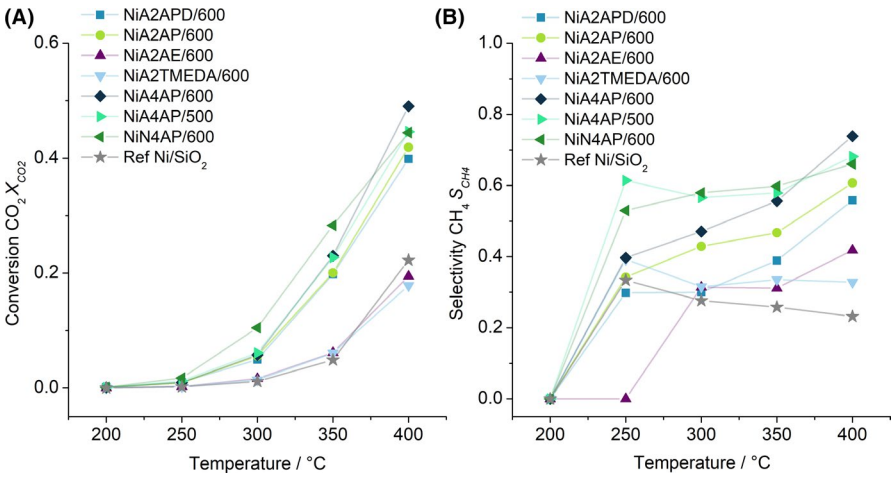


FIGURE 7 Conversion of CO_2 X_{CO_2} (A) and selectivity toward CH_4 S_{CH_4} (B) tested in CO_2 methanation for different cross-linking agents, Ni precursors, and pyrolysis temperatures [Color figure can be viewed at wileyonlinelibrary.com]

seen comparing NiA2AP/600 and NiA4AP/600. With a nickel particle size of (2.90 ± 1.91) nm NiA4AP/500 shows smaller nickel particles compared with the same composition pyrolyzed at 600°C. The smallest nickel particles and the most narrow particle distribution of (2.52 ± 0.82) nm was achieved by using NiN as nickel precursor. After the stability test of NiA4AP/600 for 10 hours at 400°C under reaction conditions a considerable increase in the particle size by a factor of 3.33 to (12.02 ± 9.96) nm can be noticed. All observed particle sizes are in the range of reported nickel catalysts prepared by other methods.[9,28–33]

Evaluation of TEM images of the reference catalyst which are shown in Figure S4 reveals a Ni particle size of (37.15 ± 28.75) nm.

3.4 | Catalytic performance

CO_2 methanation was used as probe reaction in order to investigate the applicability of nickel-containing polysiloxanes for catalytic purposes. The CO_2 conversion X_{CO_2} and the CH_4 selectivity S_{CH_4} are shown in Figure 7. Conversion as well as selectivity are maximized at the maximum reaction temperature of 400°C for all samples except for NiA2TMEDA/600 which has its maximum selectivity at 250°C. Since the thermodynamic equilibrium was not reached, the discussion of the data without considering underestimation of intrinsic activity is reasonable. Global maximum values of $C_{CO_2} = 0.49$ and $S_{CH_4} = 0.74$ are observed for NiA4AP/600. Two groups can be identified when evaluating

the conversion. For NiA2TMEDA/600 and NiA2AE/600 the conversion is very similar and exhibit with 0.18 and 0.19 the lowest measured values. In contrast, the other samples show considerable higher conversions ranging at 400°C from 0.40 for NiA2APD/600 to 0.49 for NiA4AP/600 in the order NiA2APD/600—NiA2AP/600—NiA4AP/500—NiN4AP/600—NiA4AP/600. However, at low reactions temperatures from 250°C to 350°C the sample NiN4AP/600 is clearly most effective. Following trends can be observed: the conversion increases when using AP as CLA; increasing the complexing to nickel ratio from 2 to 4 improves the activity; the pyrolysis temperature has no influence on the conversion; and finally, using NiN as nickel precursor leads to superior conversion at low temperatures.

In contrast to the conversion, clustering of samples into groups is not possible for the selectivity toward CH_4. Some trends are obvious for the selectivity: AP shows the best selectivity of all investigated CLAs and increasing the complexing group to nickel ratio. Changing the nickel precursor to NiN as well as reducing the pyrolysis temperature to 500°C leads to superior selectivity in the temperature range from 250 to 350°C. Exemplary stability test of sample NiA4AP/600 at 400°C for 10 hours under reaction conditions shows that 91% and 88% can be preserved for CO_2 conversion and CH_4 selectivity, respectively.

4 | DISCUSSION

4.1 | Influencing factors on Ni particle size

Most obviously, the pyrolysis temperature influences the nickel particle size. Higher temperatures facilitate the growth of nickel particles by diffusion and mechanisms such as Ostwald ripening. Although the pyrolysis temperature has an effect on the particle size, it is not the strongest influencing factor. The binding of Ni ions to the polymeric Si-O chain might be the reason for the comparable small increase in particle size with increasing temperature. Bazarjani et al synthesized nickel particles of 2 to 3 nm using a nickel-containing polysilazane precursor.[34] Covalent bonds of the nickel complex with the polysilazane were found. The presence of nickel has a strong impact on the resulting microstructure. By reducing the barrier for heterogeneous pore nucleation as well as reducing the viscous flow of the pores, nickel nanoparticles lead to the pronounced development of porosity (BET SSA of 215 $m^2\ g^{-1}$). Furthermore, the formation of turbostratic carbon is catalyzed by nickel.

While Bazarjani et al used polysilazanes which provide very active functional groups, in the present work relatively inactive methyl polysiloxane acts as precursor. Hence, the binding of the nickel to the polymeric network is only possible by the condensation reaction of cross-linking active OH-groups. However, this argument is only valid for samples where the functionality of complexing and cross-linking is combined in one molecule. Thus, a connection of the Ni ion to the polymeric chain can be assumed as it was reported previously.[11,13,35] This is not true for the sample NiA2TMEDA/600 where the complexing agent TMEDA has no cross-linking active groups. Consequently, binding of the complexed Ni ions to the polymeric chain is not possible. Consequently, the highest observed particle size and broadest particle size distribution among all studied samples was found for NiA2TMEDA/600. In contrast, the CLAs APD, AP, and AE provide binding of the Ni ions to the polymeric chain. Among them, AE exhibits the largest Ni particles and AP the smallest. Since each AE molecule has two complexing groups and according to the ratio complexing group/Ni of 2, each AE molecule is attributed to one Ni ion. Although two molecules of APD and AP are attributed to one Ni ion, respectively. Additionally, attribution of two AP and APD molecules to one Ni ion results in six and four cross-linking active groups per Ni, respectively. Compared with the three cross-linking active groups of AE, APD, and AP have a higher possibility to bind to the polymer chain. Furthermore, steric considerations suggest that it is more likely for AP- and APD-complexed Ni ions to get bound to the polymer chain. A better distribution of cross-linking active groups around the ion is supposed to be the reason. Apparently, not only the complexing ability but also the capability to anchor the complex to the polymer chain is an influencing factor. By comparing the particle sizes of AP ($d = (3.91 \pm 3.30)$ nm) and APD ($d = (4.94 \pm 4.42)$ nm) this becomes obvious. With three cross-linking active groups it is more likely for AP to bind to the polymer chain than it is for APD with only two groups.

Increasing the ratio of cross-linking active group to Ni from 2 to 4 in case of AP as CLA decreases the Ni particle size. Usually, the coordination number of nickel is 6. Hence, it can be assumed that an increase in the ratio from 2 to 4 in case of AP as CLA results in a more effective complexing and/or a more effective binding to the polymer chain leading to smaller nickel particles. The exact contribution of each single effect (complexing and binding) could not be clarified in this work.

Finally, also the nickel precursor influences the particle size. Organic ligands are reported to result in higher dispersion compared with nitrate in case of cobalt in impregnation methods.[19,36] On the other hand, general problems of nitrate as precursor such as sintering and redistribution of nickel during calcination causing inferior dispersion which are reported for impregnation methods are not observed for the solution-based freeze casting method.[8,19] The chelating character of the acetylacetonate anion provides the possibility for acetylacetonate to complex Ni and hence to block complexing sites even in solution. In contrast, nickel nitrate completely dissociates into ions when in solution. Consequently, complexing of Ni by the complexing

agent is facilitated for the dissociated nickel nitrate. Thus, it is more likely that nickel ions are bound to the polymeric chain when using nickel nitrate compared with nickel acetylacetonate. Furthermore, nickel acetylacetonate is composed of three nickel ions complexed by six acetylacetonate ligands. Although nickel nitrate consists of a single nickel ion. Hence, the presence of single nickel ions might be an additional reason for the better dispersion observed for nickel nitrate.

4.2 | Catalytic performance

The nickel particle size and dispersion are found to be the most influencing factors on the CO_2 conversion at a constant metal loading. The order of conversion reflects very well the order of nickel particle size with smaller nickel particles enhancing the conversion. In contrast to the findings of Macedo et al no influence of the pyrolysis temperature was found.[17] Furthermore, the increase in 50 $m^2\ g^{-1}$ in BET surface area was found to have no impact. Due to the presence of mainly micropores generating the high BET surface area, diffusion limitation of reactants in micropores can be assumed.

For CO_2 hydrogenation, it is reported that the nickel particle size has an influence on the catalytic pathway and consequently on the selectivity.[2] In this study, a trend of increasing selectivity toward CH_4 with decreasing nickel particle size was observed.

Most research found that increasing nickel size leads to higher selectivity toward CH_4 [37–39] Although, there are also studies reporting higher CO selectivity with increasing nickel size.[40] The suggested mechanism bases on the CO dissociation at highly uncoordinated sites present on steps of nickel.[41] While strong CO adsorption at edges could enable direct methanation of CO_2, nickel faces mainly produce CO. On nickel faces CO desorbs prior to methanation. Since smaller nickel particles are supposed to exhibit larger percentage of uncoordinated sites their selectivity toward CH_4 is higher. This mechanism is in accordance with studies investigating nickel on supports with weak interaction.[42,43] While supports with a strong support metal interaction such as TiO_2 and Nb_2O_5 are characterized by their reducibility, SiOC can be filed to the class of supports with weak support metal interaction such as SiO_2.[44]

The reference catalyst performs similar to the ones prepared using TMEDA and AE as cross-linking agent. The higher hydrophobicity and the smaller Ni particles of the polymer-derived catalysts are reasons for the better performance of the polymer-derived catalyst. Furthermore, the highly porous structure of the PDC sample particles shown in Figure 2H provides a higher number of accessible nickel sites compared with the dense silica particles.

The reduced conversion during the stability test is most likely due to the increased nickel size and carbon deposition.[44] Although moderate sintering is taking place, the confinement of the nickel within the matrix is supposed to help preventing severe sintering by suppressing the mobility of nickel atoms.

5 | CONCLUSIONS

Micro- and macroporous nickel-containing monoliths were prepared by solution-based freeze casting of methyl polysiloxanes. The screening of four different complexing and cross-linking siloxanes with amino functionality revealed that 3-aminopropyltriethoxysilane (AP) is most efficient in creating small and well-dispersed nickel particles. The formation of micropores due to the decomposition of organic groups of the polymer gives reason for the high BET surface area of around 400 $m^2\ g^{-1}$. Increasing the ratio of complexing groups to nickel improves the dispersion of nickel particles. The dispersion is further enhanced for changing the nickel precursor from nickel acetylacetonate to nickel nitrate. Catalytic tests of CO_2 methanation show a dependence of the CO_2 conversion and CH_4 selectivity mainly on the nickel particle size. Furthermore, selectivity toward CH_4 improves with decreasing particle size up to a value of 0.74. According to the mechanism, CO adsorption is supposed to be stronger at nickel edges, whereas on faces CO desorbs before methanation. Hence, methane generation is higher for smaller particles which exhibits more edges. Compared with nickel impregnated on silica, the polymer-derived catalysts show better conversion and selectivity. The highly porous structure of the PDC samples might provide a better mass transport compared with the impregnated catalyst.

This research shows promising catalytic activity of nickel-containing PDCs for CO_2 methanation tested in a packed bed reactor and opens up several potential approaches to further optimize monolithic metal-containing PDCs, for example, heat- and mass-transfer considerations can be easily addressed by adapting the pore structure.

ACKNOWLEDGMENTS

This work was supported by German Research Foundation (DFG) within the Research Training Group GRK 1860 “Micro-, meso-, and macroporous nonmetallic Materials: Fundamentals and Applications” (MIMENIMA). The authors thank Catherine Yokan, Nantje Steinberg, and Tuoi Hoang for experimental work.

CONFLICT OF INTEREST

The authors declare no conflict of interest.

AUTHOR CONTRIBUTIONS

Daniel Schumacher: Conceptualization, Formal analysis, Writing—original draft, Writing—review and editing, Investigation, Data curation, Visualization. Michaela Wilhelm, Kurosch Rezwan: Conceptualization, Writing—review and editing, Supervision.

ORCID

Daniel Schumacher https://orcid.org/0000-0002-3747-2410
Michaela Wilhelm https://orcid.org/0000-0001-8651-1546
Kurosch Rezwan https://orcid.org/0000-0002-7318-1119

REFERENCES

1. Su X, Xu J, Liang B, Duan H, Hou B, Huang Y. Catalytic carbon dioxide hydrogenation to methane: a review of recent studies. J Energy Chem. 2016;25(4):553–65.
2. Li W, Wang H, Jiang X, Zhu J, Liu Z, Guo X, et al. A short review of recent advances in CO_2 hydrogenation to hydrocarbons over heterogeneous catalysts. RSC Adv. 2018;8:7651–69.
3. Panagiotopoulou P, Kondarides DI, Verykios XE. Selective methanation of CO over supported noble metal catalysts: effects of the nature of the metallic phase on catalytic performance. Appl Catal A. 2008;344(1–2):45–54.
4. Aziz MAA, Jalil AA, Triwahyono S, Ahmad A. CO_2 methanation over heterogeneous catalysts: recent progress and future prospects. Green Chem. 2015;17(5):2647–63.
5. Wei W, Jinlong G. Methanation of carbon dioxide: an overview. Front Chem Sci Eng. 2010;5(1):2–10.
6. Aziz MAA, Jalil AA, Triwahyono S, Saad MWA. CO_2 methanation over Ni-promoted mesostructured silica nanoparticles: influence of Ni loading and water vapor on activity and response surface methodology studies. Chem Eng J. 2015;260:757–64.
7. Khodakov AY, Chu W, Fongarland P. Advances in the development of novel cobalt Fischer−Tropsch catalysts for synthesis of long-chain hydrocarbons and clean fuels. Chem Rev. 2007;107:1692–744.
8. Wang W, Wang S, Ma X, Gong J. Recent advances in catalytic hydrogenation of carbon dioxide. Chem Soc Rev. 2011;40(7):3703–27.
9. Yan X, Liu Y, Zhao B, Wang Z, Wang Y, Liu C-J. Methanation over Ni/SiO_2: effect of the catalyst preparation methodologies. Int J Hydrogen Energy. 2013;38(5):2283–91.
10. Zhao A, Ying W, Zhang H, Ma H, Fang D. $Ni–Al_2O_3$ catalysts prepared by solution combustion method for syngas methanation. Catal Commun. 2012;17:34–8.
11. Schubert M, Wilhelm M, Bragulla S, Sun C, Neumann S, Gesing TM, et al. The influence of the pyrolysis temperature on the material properties of cobalt and nickel containing precursor derived ceramics and their catalytic use for CO_2 methanation and Fischer-Tropsch synthesis. Catal Lett. 2017;147:472–482.
12. Wilhelm M, Adam M, Bäumer M, Grathwohl G. Synthesis and properties of porous hybrid materials containing metallic nanoparticles. Adv Eng Mater. 2008;10(3):241–5.
13. Adam M, Wilhelm M, Grathwohl G. Polysiloxane derived hybrid ceramics with nanodispersed Pt. Microporous Mesoporous Mater. 2012;151:195–200.
14. Zaheer M, Schmalz T, Motz G, Kempe R. Polymer derived non-oxide ceramics modified with late transition metals. Chem Soc Rev. 2012;41(15):5102–16.
15. Wójcik-Bania M, Krowiak A, Strzezik J, Hasik M. Pt supported on cross-linked poly(vinylsiloxanes) and SiCO ceramics—new materials for catalytic applications. Mater Des. 2016;96:171–9.
16. Schmalz T, Kraus T, Günthner M, Liebscher C, Glatzel U, Kempe R, et al. Catalytic formation of carbon phases in metal modified, porous polymer derived SiCN ceramics. Carbon. 2011;49(9):3065–72.
17. Macedo HP, Medeiros RLBA, Ilsemann J, Melo DMA, Rezwan K, Wilhelm M. Nickel-containing hybrid ceramics derived from polysiloxanes with hierarchical porosity for CO_2 methanation. Microporous Mesoporous Mater. 2019;278:156–66.
18. Naviroj M, Miller SM, Colombo P, Faber KT. Directionally aligned macroporous SiOC via freeze casting of preceramic polymers. J Eur Ceram Soc. 2015;35(8):2225–32.
19. Marceau E, Che M, Čejka J, Zukal A. Nickel(II) nitrate vs. acetate: influence of the precursor on the structure and reducibility of Ni/MCM-41 and Ni/Al-MCM-41 catalysts. ChemCatChem. 2010;2(4):413–22.
20. Liu R, Xu T, Wang C. A review of fabrication strategies and applications of porous ceramics prepared by freeze-casting method. Ceram Int. 2016;42(2):2907–25.
21. Adam M, Bäumer M, Schowalter M, Birkenstock J, Wilhelm M, Grathwohl G. Generation of Pt- and Pt/Zn-containing ceramers and their structuring as macro/microporous foams. Chem Eng J. 2014;247:205–15.
22. Adam M, Kocanis S, Fey T, Wilhelm M, Grathwohl G. Hierarchically ordered foams derived from polysiloxanes with catalytically active coatings. J Eur Ceram Soc. 2014;34(7):1715–25.
23. Vakifahmetoglu C, Zeydanli D, Colombo P. Porous polymer derived ceramics. Mater Sci Eng, R. 2016;106:1–30.
24. Colombo P. Engineering porosity in polymer-derived ceramics. J Eur Ceram Soc. 2008;28(7):1389–95.
25. Prenzel T, Wilhelm M, Rezwan K. Pyrolyzed polysiloxane membranes with tailorable hydrophobicity, porosity and high specific surface area. Microporous Mesoporous Mater. 2013;169:160–7.
26. Zhang H, Fidelis CL, Serva ALT, Wilhelm M, Rezwan K. Water-based freeze casting: adjusting hydrophobic polymethylsiloxane for obtaining hierarchically ordered porous SiOC. J Am Ceram Soc. 2017;100:1907–1918.
27. Schumacher D, Wilhelm M, Rezwan K. Modified solution based freeze casting process of polysiloxanes to adjust pore morphology and surface functions of SiOC monoliths. Mater Des. 2018;160:1295–304.
28. He S, Zheng X, Mo L, Yu W, Wang H, Luo Y. Characterization and catalytic properties of Ni/SiO_2 catalysts prepared with nickel citrate as precursor. Mater Res Bull. 2014;49:108–13.
29. Liu D, Wang Y, Shi D, Jia X, Wang X, Borgna A, et al. Methane reforming with carbon dioxide over a $Ni/ZiO_2–SiO_2$ catalyst: influence of pretreatment gas atmospheres. Int J Hydrogen Energy. 2012;37(13):10135–44.
30. Li L, He S, Song Y, Zhao J, Ji W, Au C-T. Fine-tunable Ni@porous silica core–shell nanocatalysts: synthesis, characterization, and catalytic properties in partial oxidation of methane to syngas. J Catal. 2012;288:54–64.
31. Bykova MV, Ermakov DYU, Kaichev VV, Bulavchenko OA, Saraev AA, Lebedev MYU, et al. Ni-based sol–gel catalysts as promising systems for crude bio-oil upgrading: guaiacol hydrodeoxygenation study. Appl Catal B. 2012;113–114:296–307.
32. Xue M, Hu S, Chen H, Fu Y, Shen J. Preparation of highly loaded and dispersed Ni/SiO_2 catalysts. Catal Commun. 2011;12(5):332–6.
33. Xia W-S, Hou Y-H, Chang G, Weng W-Z, Han G-B, Wan H-L. Partial oxidation of methane into syngas (H2 + CO) over effective

high-dispersed Ni/SiO_2 catalysts synthesized by a sol–gel method. Int J Hydrogen Energy. 2012;37(10):8343–53.

34. Seifollahi Bazarjani M, Kleebe H-J, Müller MM, Fasel C, Baghaie Yazdi M, Gurlo A, et al. Nanoporous silicon oxycarbonitride ceramics derived from polysilazanes in situ modified with nickel nanoparticles. Chem Mater. 2011;23(18):4112–23.
35. Gorschinski A, Khelashvili G, Schild D, Habicht W, Brand R, Ghafari M, et al. A simple aminoalkyl siloxane-mediated route to functional magnetic metal nanoparticles and magnetic nanocomposites. J Mater Chem. 2009;19:2289–38.
36. Śrębowata A, Juszczyk W, Kaszkur Z, Sobczak JW, Kępiński L, Karpiński Z. Hydrodechlorination of 1,2-dichloroethane and dichlorodifluoromethane over Ni/C catalysts: the effect of catalyst carbiding. Appl Catal A. 2007;319:181–92.
37. Wu HC, Chang YC, Wu JH, Lin JH, Lin IK, Chen CS. Methanation of CO_2 and reverse water gas shift reactions on Ni/SiO_2 catalysts: the influence of particle size on selectivity and reaction pathway. Catal Sci Tech. 2015;5(8):4154–63.
38. Kwak JH, Kovarik L, Szanyi J. CO_2 reduction on supported Ru/Al_2O_3 catalysts: cluster size dependence of product selectivity. ACS Catalysis. 2013;3(11):2449–55.
39. Kwak JH, Kovarik L, Szanyi J. Heterogeneous catalysis on atomically dispersed supported metals: CO_2 reduction on multifunctional Pd catalysts. ACS Catalysis. 2013;3(9):2094–100.
40. Garbarino G, Riani P, Magistri L, Busca G. A study of the methanation of carbon dioxide on Ni/Al_2O_3 catalysts at atmospheric pressure. Int J Hydrogen Energy. 2014;39(22):11557–65.
41. Engbæk J, Lytken O, Nielsen JH, Chorkendorff I. CO dissociation on Ni: the effect of steps and of nickel carbonyl. Surf Sci. 2008;602(3):733–43.
42. Aziz MAA, Jalil AA, Triwahyono S, Mukti RR, Taufiq-Yap YH, Sazegar MR. Highly active Ni-promoted mesostructured silica nanoparticles for CO_2 methanation. Appl Catal B. 2014;147:359–68.
43. Aldana PAU, Ocampo F, Kobl K, Louis B, Thibault-Starzyk F, Daturi M, et al. Catalytic CO_2 valorization into CH_4 on Ni-based ceria-zirconia. Reaction mechanism by operando IR spectroscopy. Catal Today. 2013;215:201–7.
44. Fu Q, Wagner T. Interaction of nanostructured metal overlayers with oxide surfaces. Surf Sci Rep. 2007;62:431–98.

SUPPORTING INFORMATION

Additional supporting information may be found online in the Supporting Information section.

How to cite this article: Schumacher D, Wilhelm M, Rezwan K. Porous SiOC monoliths with catalytic activity by in situ formation of Ni nanoparticles in solution-based freeze casting. *J Am Ceram Soc*. 2020;103:2991–3001. https://doi.org/10.1111/ace.16988